LETTERS
PUBLISHED ONLINE: 17 JULY 2011 | DOI: 10.1038/NMAT3074
nature materials

Maltodextrin-based imaging probes detect bacteria *in vivo* with high sensitivity and specificity

Xinghai Ning[1†], Seungjun Lee[1†], Zhirui Wang[2], Dongin Kim[1], Bryan Stubblefield[3], Eric Gilbert[3] and Niren Murthy[1*]

The diagnosis of bacterial infections remains a major challenge in medicine. Although numerous contrast agents have been developed to image bacteria, their clinical impact has been minimal because they are unable to detect small numbers of bacteria *in vivo*, and cannot distinguish infections from other pathologies such as cancer and inflammation[1–7]. Here, we present a family of contrast agents, termed maltodextrin-based imaging probes (MDPs), which can detect bacteria *in vivo* with a sensitivity two orders of magnitude higher than previously reported, and can detect bacteria using a bacteria-specific mechanism that is independent of host response and secondary pathologies. MDPs are composed of a fluorescent dye conjugated to maltohexaose, and are rapidly internalized through the bacteria-specific maltodextrin transport pathway[8–11], endowing the MDPs with a unique combination of high sensitivity and specificity for bacteria. Here, we show that MDPs selectively accumulate within bacteria at millimolar concentrations, and are a thousand-fold more specific for bacteria than mammalian cells. Furthermore, we demonstrate that MDPs can image as few as 10^5 colony-forming units *in vivo* and can discriminate between active bacteria and inflammation induced by either lipopolysaccharides or metabolically inactive bacteria.

Bacterial infections cause significant mortality and morbidity worldwide despite the availability of antibiotics. For example, in the United States in 2010, bacterial infections caused 40,000 deaths from sepsis alone and were also the leading cause of limb amputations[12,13]. A major limitation preventing the effective treatment of bacterial infections is an inability to image them *in vivo* with accuracy and sensitivity. Consequently, bacterial infections can be diagnosed only after they have become systemic or have caused significant anatomical tissue damage, a stage at which they are challenging to treat owing to the high bacterial burden[14,15]. There is therefore a great need for the development of contrast agents that can image small numbers of bacteria accurately *in vivo*.

Here we present a family of contrast agents that are robustly internalized through the bacteria-specific maltodextrin transporter and can image bacterial infections *in vivo* with unprecedented sensitivity and specificity (see Fig. 1). Maltohexaose is a major source of glucose for bacteria[16] and MDPs can therefore deliver millimolar concentrations of imaging probes into bacteria, making it possible to image low numbers of bacteria. MDPs also have high specificity for bacteria because mammalian cells do not express the maltodextrin transporter[9] and cannot internalize contrast agents conjugated to maltohexaose. MDPs are composed of α (1–4)-linked glucose oligomers, which are hydrophilic and membrane impermeable[17]; therefore, MDPs are efficiently cleared from uninfected tissues *in vivo*, leading to a low background. Furthermore, the lumen of intestinal tissues or the outer layers of the skin are not permeable to glucose oligomers[18], and MDPs delivered systemically should therefore not be internalized by the resident bacterial microflora present in healthy subjects. These unique properties should allow MDPs to accurately and sensitively image bacteria *in vivo*.

The bacterial imaging agents MDP-1 and MDP-2 were synthesized to image bacteria *in vitro* and *in vivo*, and are composed of maltohexaose conjugated to either perylene or IR786 (see Fig. 2). MDP-1 and MDP-2 were synthesized by clicking alkyne-functionalized fluorescent dyes onto an azide-functionalized maltohexaose[19,20], which was synthesized from maltohexaose in four steps, following the scheme shown in the Supplementary Information. This synthetic strategy introduces the imaging probes at the anomeric carbon of maltohexaose and was selected because maltodextrin transporters tolerate structural modifications at the reducing end of maltodextrins[21,22].

A central problem in imaging bacterial infections is to develop targeting strategies that can deliver large quantities of imaging probes to bacteria. This has been challenging because most present imaging probes target the bacterial cell wall and cannot access the bacterial intracellular volume[2–5]. Maltodextrin transporters, in contrast, internalize their substrates at a robust rate and MDPs should therefore be capable of reaching a high concentration within bacteria. We therefore investigated the uptake of MDP-1 in gram-positive and gram-negative bacteria, under aerobic and anerobic fermentative conditions. *Escherichia coli*, *Pseudomonas aeruginosa*, *Bacillus subtilis* and *Staphylococcus aureus* were incubated with a 20 μM concentration of MDP-1 for 1 h, washed with PBS, lysed, and the MDP-1 in the cellular supernatant was analysed by fluorescence microscopy. Figure 3a demonstrates that MDPs can deliver large quantities of imaging probes to bacteria, under both aerobic and anaerobic fermentative conditions (see Supplementary Fig. S11). For example, *E. coli* internalized MDP-1 at a rate sufficient to generate millimolar intracellular concentrations, and followed Michaelis–Menten kinetics, with a V_{max} of 2.7 nmol min^{-1} per 10^9 cells and a K_M of 1.3 μM (shown in Fig. 3b). Furthermore, pathogenic bacteria such as *P. aeruginosa*, *S. aureus* and *B. subtilis* also robustly internalized MDP-1. To our

[1]The Wallace H. Coulter Department of Biomedical Engineering and the Parker H. Petit Institute for Bioengineering and Bioscience, Georgia Institute of Technology, Atlanta, Georgia 30332, USA, [2]Complex Carbohydrate Research Center, University of Georgia, Athens, Georgia 30602, USA, [3]Department of Biology, Georgia State University, Atlanta, Georgia 30302, USA. †These authors contributed equally to this work. *e-mail: niren.murthy@bme.gatech.edu.

© 2011 Macmillan Publishers Limited. All rights reserved

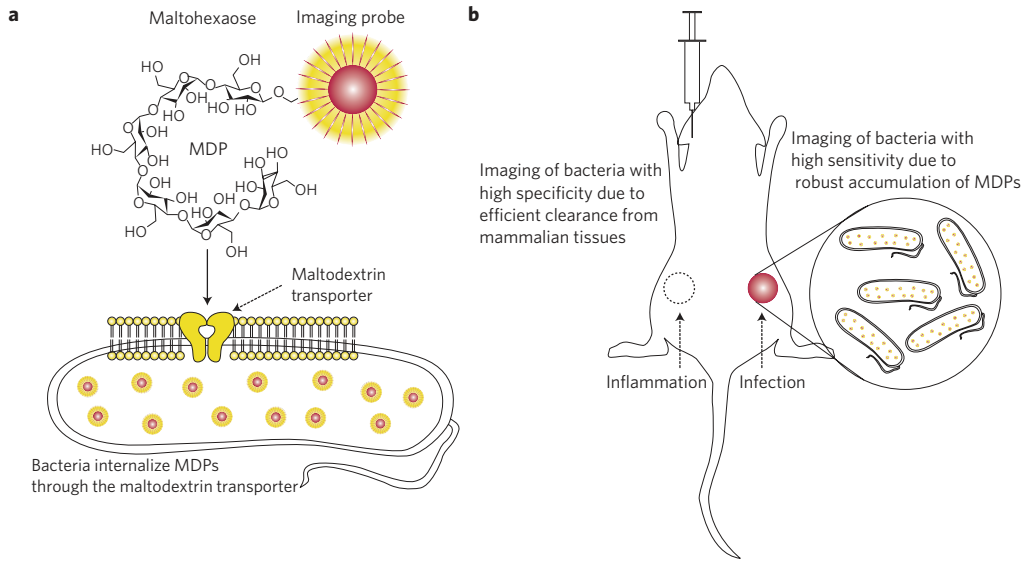

Figure 1 | *In vivo* detection of bacteria with MDPs. a, Chemical design of MDPs. MDPs are a family of contrast agents that target the maltodextrin transport pathway and can image bacteria *in vivo*. MDPs are composed of maltohexaose conjugated to an imaging probe. MDPs are internalized as a glucose source and are transported by bacteria at a high rate. Maltodextrin transporters are not present in mammalian cells and MDPs therefore also have specificity for bacteria. **b**, MDPs image bacteria *in vivo* with high sensitivity and specificity. MDPs are robustly internalized by bacteria but not by mammalian cells, and can therefore detect low numbers of bacteria *in vivo* and also distinguish between inflammation and bacterial infections.

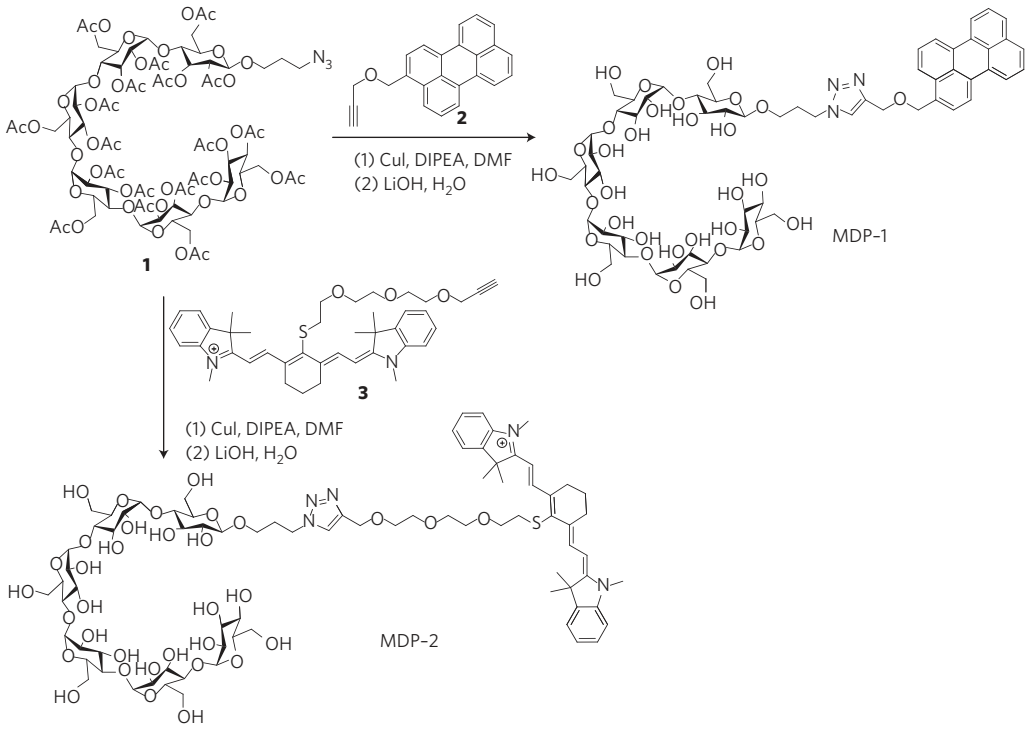

Figure 2 | Synthesis of MDP-1 and MDP-2. MDP-1 and MDP-2 were synthesized by conjugation of **1** with either **2** or **3** using the copper (I) catalysed click reaction.

knowledge, this represents the first demonstration of a targeting strategy that can deliver millimolar concentrations of an imaging probe to bacteria.

We performed experiments with LamB mutant *E. coli* (LamB mutants)[23] to determine whether MDP-1 was internalized through the maltodextrin transporter. LamB mutants were incubated with MDP-1 and the internalization of MDP-1 was determined following the procedure described above. Figure 3a demonstrates that LamB mutants do not internalize MDP-1 and that, therefore, MDP-1 enters *E. coli* through the maltodextrin transport pathway. The uptake of MDP-1 in wild-type *E. coli* could also be inhibited by an excess of maltose or maltohexaose, further confirming that MDP-1 is internalized by maltodextrin transporters (see Supplementary Fig. S12). Finally, we investigated whether metabolically inactive bacteria (azide-treated) internalized MDP-1. Figure 3a shows that metabolically inactive bacteria do not accumulate MDP-1, demonstrating that MDP-1 is not binding to the bacteria cell surface through non-specific interactions.

© 2011 Macmillan Publishers Limited. All rights reserved

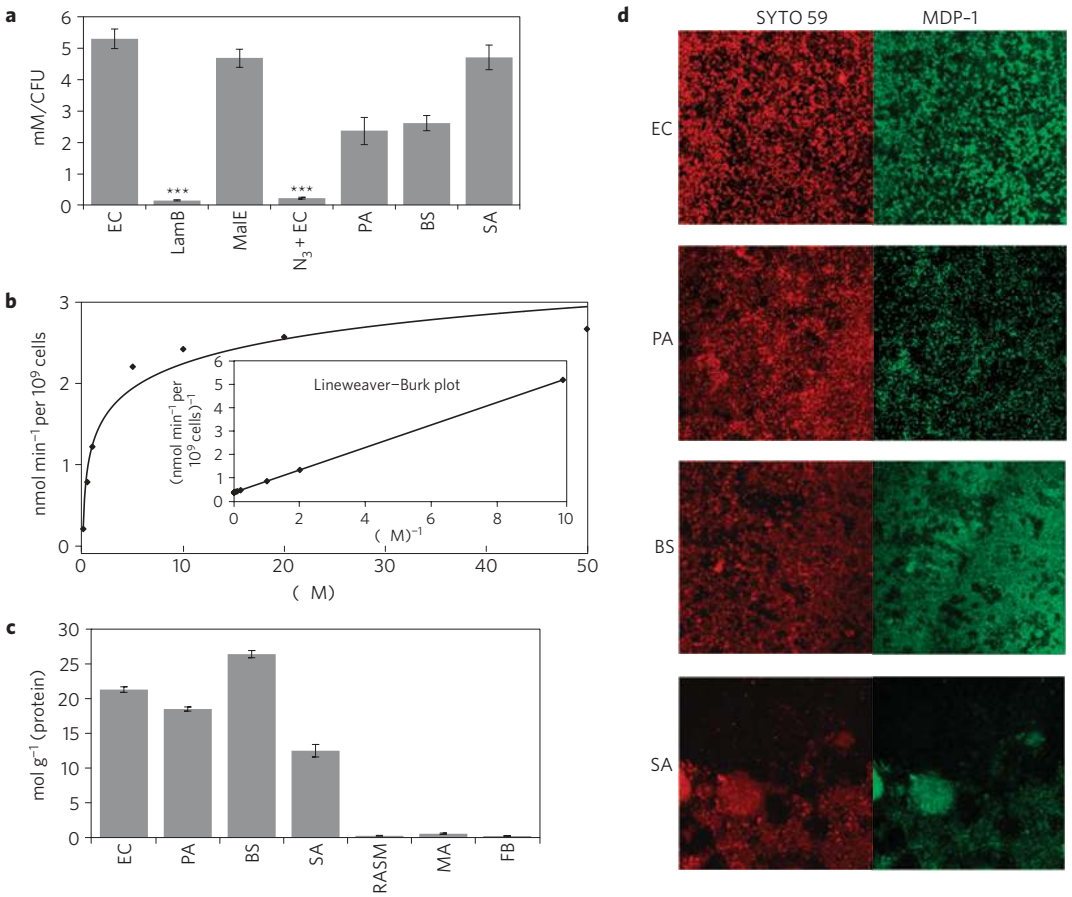

Figure 3 | MDPs have specificity for planktonic bacteria and bacterial biofilms. a, Histogram showing the levels of MDP-1 internalization. Gram-negative and gram-positive bacteria robustly internalize MDP-1. MDP-1 is robustly internalized by *E. coli* (EC), *P. aeruginosa* (PA), *B. subtilis* (BS), *S. aureus* (SA) and *E. coli* MalE mutant strains (MalE). The uptake of MDP-1 in *E. coli* LamB mutant strains (LamB) and metabolically inactive *E. coli* (EC + N_3) is significantly reduced. Results are expressed as mean millimolar concentration per CFU ± standard error of the mean (s.e.m.), for $n = 6$ per group. The p values between the EC and LamB or EC + N_3 were determined by a one-way analysis of variance (ANOVA) using Bonferroni's post-hoc test, and were found to be statistically significant ($p \leq 0.001$). **b**, Plot showing that the uptake of MDP-1 in *E. coli* is saturable and follows Michaelis–Menten kinetics, with a V_{max} of 2.7 nmol min $^{-1}$ per 10^9 cells and a K_M of 1.3 μM. **c**, Histogram quantifying the level of MDP-1 transport. MDP-1 has high specificity for bacteria when compared with mammalian cells. Bacteria (*E. coli*, *P. aeruginosa*, *B. subtilis* and *S. aureus*) transport MDP-1 at a rate three orders of magnitude faster than mammalian cells (rat aortic smooth muscle cells (RASMs), macrophages (MAs) and fibroblasts (FBs)). The results are expressed as mean micromoles per gram of protein ± s.e.m. for $n = 6$ per group. The p values between each group of bacteria and each group of mammalian cells were determined by a one-way ANOVA using Bonferroni's post-hoc test, and were found to be statistically significant ($p \leq 0.001$). **d**, Fluorescence micrographs showing that the biofilms (*E. coli*, *P. aeruginosa*, *B. subtilis* and *S. aureus*) robustly internalize MDP-1.

A key challenge in imaging bacteria is to develop probes that have high specificity for bacteria. For example, several present bacterial imaging agents detect bacterial infections using mechanisms that have previously been employed to image inflammation or cancer, and thus lack specificity[1–3,5]. Present imaging strategies therefore have a high rate of false positives and require an invasive biopsy for verification. In contrast, MDPs have the potential to image bacteria with high specificity because mammalian cells do not express maltodextrin transporters[9]. MDPs should also have low levels of non-specific uptake in mammalian cells because they are hydrophilic and cannot pentrate the membrane[17]. We therefore investigated the specificity of MDPs towards bacteria. The uptake of MDPs in bacteria and mammalian cells was determined and compared. Bacteria (*E. coli*, *P. aeruginosa*, *B. subtilis* and *S. aureus*) and mammalian cells (rat aortic smooth muscle cells, macrophages and fibroblasts) were incubated with a 20 μM concentration of MDP-1 for 1 h, washed with PBS, lysed, and the cellular supernatant was analysed for perylene fluorescence signal. Figure 3c shows that MDP-1 has high specificity for bacteria. For example, both gram-positive and gram-negative bacteria internalized MDP-1 at a rate three orders of magnitude faster than mammalian cells. In particular, pathogenic bacteria such as *P. aeruginosa* and *S. aureus* internalized 200–300 μmol of MDP-1 per milligram of protein, whereas rat aortic smooth muscle cells and fibroblasts internalized undetectable levels of MDP-1. Furthermore, MDP-2 has a similarly high level of specificity for bacteria when compared with mammalian cells (see Supplementary Fig. S9). We found that MDPs have a thousand times better selectivity for bacteria when compared with mammalian cells and should therefore be able to detect bacteria *in vivo* with high specificity.

We performed experiments to determine whether MDPs could target bacterial biofilms, a major source of pathology from infectious diseases[24–27]. Although bacterial biofilms have a significantly altered physiology in comparison with planktonic bacteria, they still consume glucose, and therefore can potentially be imaged by MDPs. We therefore investigated the ability of MDP-1 to image bacterial biofilms. Biofilms were incubated with a 20 μM concentration of MDP-1 for 10 min, and counter-stained with SYTO59, a long-wavelength cell-permeable nucleic acid stain. Figure 3d demonstrates that MDP-1 is actively taken up by a wide

© 2011 Macmillan Publishers Limited. All rights reserved

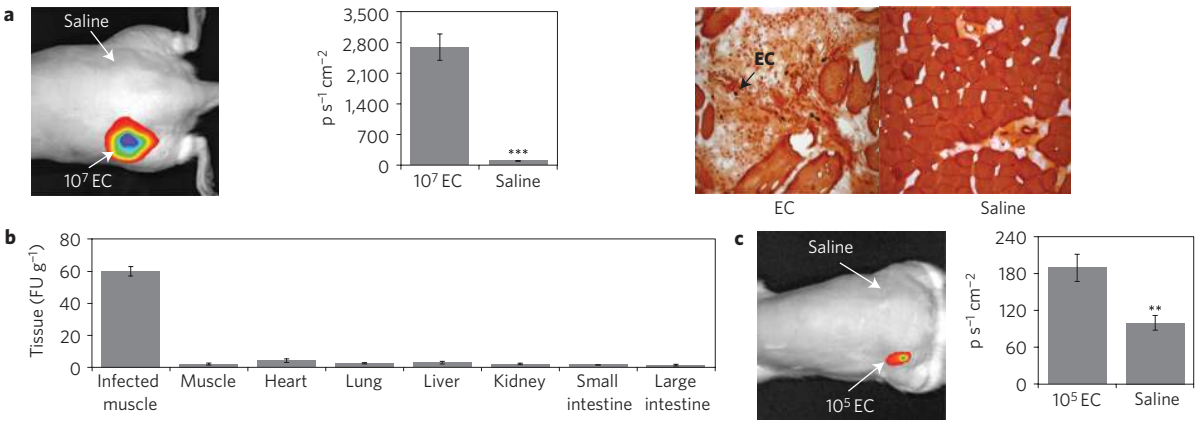

Figure 4 | MDP-2 images bacteria *in vivo*. a Left: fluorescence image of a rat showing that MDP-2 can image 10^7 *E. coli* CFUs *in vivo*. Middle: histogram showing quantification of fluorescence intensity. *E. coli* (10^7 CFUs) infected muscles have a 26-fold increase in fluorescence intensity when compared with uninfected control muscles. Right: micrograph of the histology of *E. coli*-injected thigh muscles showing that bacteria are present in infected muscles (×20 magnification). **b**, Histogram showing MDP-2 distribution in rats infected with *E. coli*. MDP-2 is efficiently cleared from all the major organs and selectively accumulates in infected muscle tissue. Data are plotted as mean fluorescent units (FUs) per gram of tissue ± s.e.m. ($n = 6$ rats per group). The p values between the infected muscle and the other tissues were determined by a one-way ANOVA using Bonferroni's post-hoc test, and were found to be statistically significant ($p \leq 0.001$). **c** Left: fluorescence image of a rat showing that MDP-2 can image 10^5 *E. coli* CFUs *in vivo*. Right: histogram showing quantification of fluorescence intensity. *E. coli* (10^5 CFUs) infected muscles have a twofold increase in fluorescence intensity when compared with uninfected control muscles. The rat images in **a** left and **c** left are representative results of six experiments. Regions of interest (ROI) in **a** left and **c** left were identified and integrated using software from the Lumina machine. The results in **a** middle and **c** middle are expressed as mean numbers of photons per second per cm^2 in the designated ROI ± s.e.m. for $n = 6$ per group. The statistical significances in **a** middle and **c** middle were determined using a two-sample Student t-test (**$p \leq 0.01$ and ***$p \leq 0.001$).

variety of bacterial biofilms. In particular, biofilms formed from *E. coli* (12 ± 4 μm thickness), *P. aeruginosa* (24 ± 15 μm thickness), *B. subtilis* (16 ± 7 μm thickness) and *S. aureus* (51 ± 30 μm thickness) all avidly internalized MDP-1, demonstrating that maltodextrin transporters are active in bacterial biofilms and can potentially be used in diagnosing diseases associated with bacterial biofilms.

On the basis of these *in vitro* results we formed a hypothesis that MDPs have the potential to image bacteria *in vivo*. Accordingly, we investigated the ability of MDP-2 to image bacterial infections in rats. The rats were injected in the left and right thigh muscles, respectively, with *E. coli* (10^7 colony-forming units, CFUs) and saline (as a control). After 1 h the rats were injected with MDP-2 (280–350 μl of 1 mM MDP-2 in PBS) through the jugular vein and imaged after 16 h in an IVIS imaging machine. Figure 4a shows that MDP-2 can image bacterial infections *in vivo*. For example, rat thigh muscles infected with *E. coli* had a 26-fold increase in fluorescence intensity when compared with uninfected controls, allowing the infected area to be easily visualized *in vivo*. We further quantified the ability of MDP-2 to target bacteria *in vivo* by performing a biodistribution study of MDP-2 in rats infected with *E. coli* (10^7 CFUs). Figure 4b demonstrates that MDP-2 accumulates in infected muscle tissues and is efficiently cleared from uninfected muscle, having a 42-fold increase in fluorescence intensity between infected and uninfected muscle tissues. MDP-2 did not accumulate in the bacterial microflora of colon tissue, presumably because of the impermeability of the lumen tissue of intestinal tissues to glucose oligomers[18]. MDP-2 was also efficiently cleared from all the major organs, indicating that it could potentially be used for imaging infections in a wide range of tissues.

We also performed experiments to determine the minimum number of bacteria that could be detected by MDP-2 *in vivo*. *E. coli* (10^5 CFUs) were injected into the left rear thigh muscle of rats and imaged with MDP-2 as described above. Figure 4c demonstrates that MDP-2 is capable of detecting as few as 10^5 bacterial CFUs *in vivo*. For example, rat thigh muscles infected with 10^5 bacterial CFUs had a twofold increase in fluorescence intensity when compared with uninfected controls. Present contrast agents for imaging bacteria, such as FIAU (ref. 1), zinc-dipicolylamine probes[2] and antimicrobial peptides[4], can image only 10^7–10^8 bacterial CFUs *in vivo*; in comparison MDP-2 has a two orders of magnitude higher sensitivity for bacteria *in vivo*.

Finally, we investigated the specificity of MDP-2 for bacteria *in vivo*. The development of contrast agents that have high specificity for bacteria has been challenging because most contrast agents also accumulate in inflamed and cancerous tissues[1–3,5], owing to their increased metabolic activity and permeability. In contrast, MDP-2 has a thousandfold specificity for bacteria when compared with mammalian cells and clears well from uninfected tissues; therefore, it has the potential to image bacteria with high specificity *in vivo*. We performed experiments to determine whether MDP-2 could distinguish bacterial infections from both lipopolysaccharide (LPS)-induced inflammation[28] and inflammation induced by metabolically inactive bacteria[29]. We also performed experiments with LamB mutants[23] to determine whether MDP-2 internalization *in vivo* was occurring by transport through the maltodextrin transporter.

We injected rats with 10^7 CFUs of *E. coli* in the left thigh muscle and either LPS (1 mg kg^{-1}) or metabolically inactive *E. coli* in the right thigh muscle, and then imaged them using MDP-2 as described above. Figure 5a shows that MDP-2 can distinguish between bacterial infections and inflammation with high specificity. For example, rat thigh muscles infected with *E. coli* had a 17-fold increase in fluorescence intensity when compared with LPS-treated tissues. Furthermore, MDP-2 did not accumulate in metabolically inactive *E. coli* (Fig. 5b), demonstrating that MDP-2 is being actively transported by bacteria *in vivo*. Finally, we investigated whether MDP-2 was being internalized *in vivo* through the maltodextrin transporter. LamB mutants (10^7 CFUs) were injected into rats and the uptake of MDP-2 was compared with that for wild-type *E. coli*, as described above. Figure 5c demonstrates that LamB mutants did not internalize MDP-2, indicating that MDP-2 is transported *in vivo* through the maltodextrin transport pathway. The uptake of MDP-2 in *E. coli* could also be inhibited by an excess of maltose *in vivo*, further confirming that MDP-2 is being internalized by maltodextrin transporters (see Supplementary Fig. S16).

© 2011 Macmillan Publishers Limited. All rights reserved

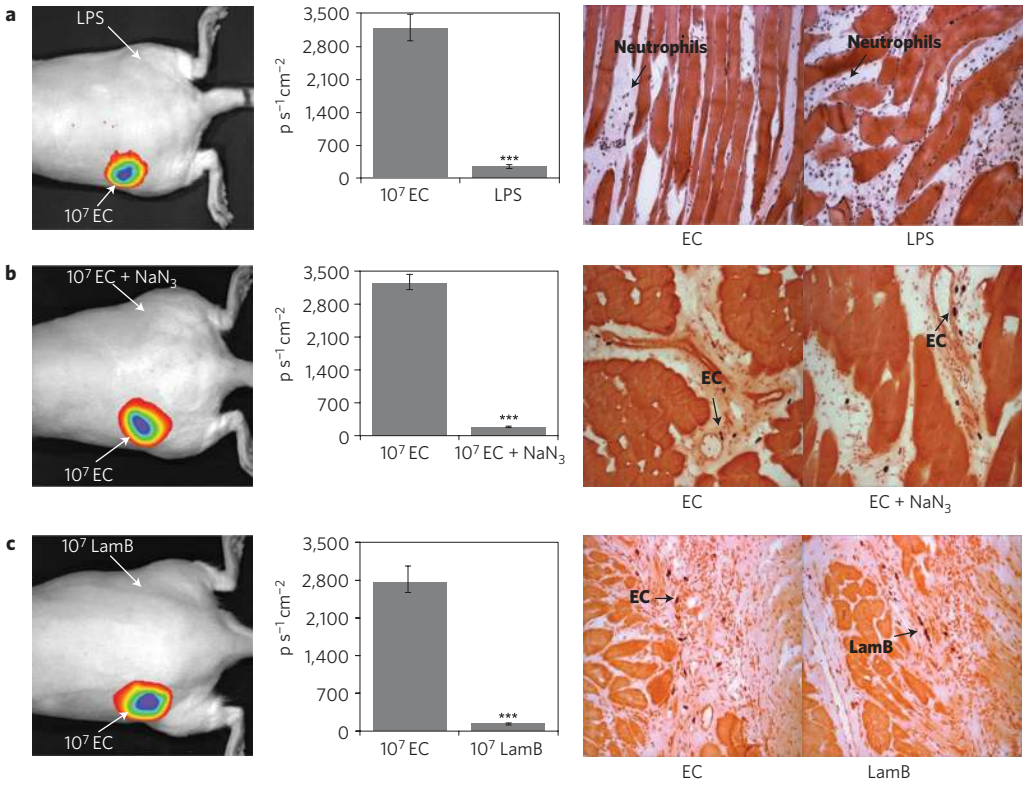

Figure 5 | MDP-2 images bacteria *in vivo* using internalization through the maltodextrin transporter. a Left: image showing that MDP-2 can distinguish between *E. coli* infection (10^7 CFUs) and LPS (1 mg kg^{-1})-induced inflammation. Middle: histogram showing quantification of fluorescence intensity. *E. coli*-infected tissues had a 17-fold increase in fluorescence intensity when compared with LPS-treated tissues. Right: micrograph showing the histology of *E. coli*- and LPS-treated muscles demonstrating that both *E. coli* and LPS induce a large amount of inflammation (×20 magnification). **b** Left: image showing that MDP-2 is actively transported by bacteria *in vivo*, and does not accumulate in metabolically inactive bacteria. Middle: histogram showing quantification of fluorescence intensity. *E. coli*-infected tissues have an 18-fold increase in fluorescence intensity when compared with tissues treated with metabolically inactive bacteria. Right: image showing the histology of thigh muscles injected with either *E. coli* or metabolically inactive *E. coli* demonstrating that bacteria are present (×20 magnification). **c** Left: image showing that MDP-2 is transported by bacteria *in vivo*, through the maltodextrin transport pathway, and does not accumulate in LamB mutants. Middle: histogram showing quantification of fluorescence intensity. *E. coli*-infected tissues have a 20-fold increase in fluorescence intensity when compared with tissues treated with LamB-negative *E. coli*. Right: image showing histology of thigh muscles injected with either *E. coli* or LamB mutants demonstrating that bacteria are present in infected muscles (×20 magnification). The rat images in **a** left, **b** left and **c** left are representative results of six experiments. Regions of interest in **a** left, **b** left and **c** left were identified and integrated using software from the Lumina machine. The results in **a** middle, **b** middle and **c** middle are expressed as mean numbers of photons per second per cm^2 in the designated ROI ± s.e.m. for $n = 6$ per group. The statistical significances in **a** middle, **b** middle and **c** middle were determined using a two-sample Student *t*-test (***$p \leq 0.001$).

There is a great need to develop contrast agents that can image bacterial infections with high sensitivity and specificity. In this report we demonstrate that MDPs have a unique combination of robust transport and high specificity, and are able to detect as few as 10^5 CFUs *in vivo* with high specificity. MDPs have tremendous potential for improving the diagnosis of bacterial infections, given their ability to accurately detect small numbers of bacteria *in vivo*.

Methods

Synthesis of MDP-1 and MDP-2. See Fig. 2. MDP-1 and MDP-2 were synthesized by conjugating alkyne-functionalized fluorescent dyes **2** and **3** to azide-functionalized maltohexaose **1**, using the click reaction. The synthesis and characterization of the intermediates **1**, **2** and **3** are described in the Supplementary Information. The details of the click reaction between **1** and **3** used to generate MDP-2 are described below. The compounds **1** (57.0 mg, 0.03 mmol) and **3** (39.0 mg, 0.06 mmol) were dissolved in DMF (5 ml), to which was added CuI (0.6 mg, 3.0 μmol) and DIPEA (1.2 mg, 0.01 mmol). The mixture was stirred at room temperature for 24 h under nitrogen and the solvent was removed *in vacuo*. The residue was redissolved in CH_2Cl_2 (20 ml) and washed with water (5 ml) and brine (5 ml). The organic phase was dried over Na_2SO_4, filtered and evaporated to dryness *in vacuo*. The residue was purified by flash column chromatography on silica gel (CH_2Cl_2/CH_3OH, 15/1) to afford the intermediate **15** in a 73% yield (55.0 mg, see Supplementary Information for structure and characterization). This intermediate **15** (50.0 mg, 0.02 mmol) was deprotected in a mixture of CH_3OH (2 ml) and aqueous LiOH (1.0 M, 2 ml) for 24 h under nitrogen. The crude MDP-2 was isolated by neutralizing the reaction mixture with Dowex 50W resin, filtering, and concentrating *in vacuo*. MDP-2 was purified by flash column chromatography on silica gel ($CH_2Cl_2/CH_3OH/H_2O$, 5/5/2) (33.8 mg, quantitative). See Supplementary Information for characterization of MDP-2 and details of the synthesis and characterization of MDP-1.

Uptake of MDP-1 and MDP-2 *in vitro*. Uptake of MDP-1 and MDP-2 in bacteria (Fig. 3 and Supplementary Fig. S9, respectively).

The uptake of MDP-1 and MDP-2 was investigated in *E. coli* (ATCC 33456), *P. aeruginosa* (ATCC 47085), *B. subtilis* (ATCC 23059), *S. aureus* (ATCC 6538), metabolically inactive *E. coli* (sodium azide-treated, see details in the Supplementary Information) and two *E. coli* mutant strains, which contained either a LamB mutation (JW3992-1) or a MalE mutation (TL212; ref. 30). All bacteria were cultured overnight in Luria–Bertani medium at 37 °C under 5% CO_2 in an incubator shaker (Innova 4230, New Brunswick Scientific). Bacteria (100 μl from the overnight culture) were re-suspended in 30 ml fresh Luria–Bertani medium and cultured to an attenuance $D_{600nm} = 0.5$ in a 250 ml flask in an incubator shaker. Bacteria (3 ml) at steady-state growth were transferred into six-well plates and incubated with 20 μM MDP-1 or MDP-2 in Luria–Bertani medium in an incubator shaker at 37 °C for 1 h. The bacteria were centrifuged at 10,000 r.p.m. for 15 min in 15 ml centrifuge tubes, using a Microfuge 18 centrifuge (Beckman Coulter). The recovered bacterial pellets were washed three times with 10 ml PBS. The bacteria were lysed in 2 ml deionized water by sonication with a Branson Sonifier S-250A (Branson Ultrasonics Corporation), using a constant duty cycle at a 200 W output; 10 sonication cycles were performed. The bacterial supernatant (diluted in a 2 ml

© 2011 Macmillan Publishers Limited. All rights reserved

volume) was isolated by centrifuging at 10,000 r.p.m. for 10 min. The fluorescence intensity of the supernatant was measured in a Shimadzu spectrofluorometer (RF 5301PC) and normalized to either the bacterial protein content or the bacterial cell volume. See Supplementary Information for detailed procedures.

Uptake of MDP-1 in bacterial biofilms. See Fig. 3d. The uptake of MDP-1 in bacterial biofilms is described in the Supplementary Information.

***In vivo* imaging of bacterial infections with MDP-2.** *In vivo* imaging of 10^5–10^7 bacterial CFUs (Fig. 4 and Supplementary Fig. S14).

Female Wistar rats (10 weeks, 200–250 g, Harlan Laboratories) were anaesthetized with isofluorane and the hair on the thigh and back was removed. A suspension of *E. coli* (10^5–10^7 CFUs) in 250 μL saline was injected into the left rear thigh muscle (injection depth 5 mm), and 250 μL of saline was injected into right rear thigh muscle as a control (injection depth 5 mm). After 1 h the rats were injected with MDP-2 (280–350 μL of 1 mM MDP-2 in PBS) through the jugular vein. Fluorescence images were captured using an IVIS Lumina Imaging System (Caliper Life Sciences) 16 h after the MDP-2 injection. The fluorescence intensity from the bacteria or saline injection area (region of interest) was integrated. At the end of the imaging procedure rats were euthanized, by CO_2 inhalation, and the bacterial infected and saline-treated muscles were collected and analysed by histology for the presence of bacteria. See Supplementary Information for detailed procedures. Six rats were used for each experimental group.

Animal protocol. All animal studies were conducted under an animal protocol that was approved by the Animal Use and Care Committee of the Georgia Institute of Technology (IACUC # A10041).

Received 5 January 2011; accepted 16 June 2011; published online 17 July 2011

References

1. Bettegowda, C. *et al.* Imaging bacterial infections with radiolabeled 1-(2′-deoxy-2′-fluoro-β-D-arabinofuranosyl)-5-iodouracil. *Proc. Natl Acad. Sci. USA* **102,** 1145–1150 (2005).
2. Leevy, W. M. *et al.* Optical imaging of bacterial infection in living mice using a fluorescent near-infrared molecular probe. *J. Am. Chem. Soc.* **128,** 16476–16477 (2006).
3. Smith, B. A. *et al.* Optical imaging of mammary and prostate tumors in living animals using a synthetic near infrared zinc(II)-dipicolylamine probe for anionic cell surfaces. *J. Am. Chem. Soc.* **132,** 67–69 (2010).
4. Welling, M. M., Paulusma-Annema, A., Balter, H. S., Pauwels, E. K. & Nibbering, P. H. Technetium-99m labelled antimicrobial peptides discriminate between bacterial infections and sterile inflammations. *Eur. J. Nucl. Med.* **27,** 292–301 (2000).
5. Mahfouz, T. *et al.* ^{18}F-fluorodeoxyglucose positron emission tomography contributes to the diagnosis and management of infections in patients with multiple myeloma: A study of 165 infectious episodes. *J. Clin. Oncol.* **23,** 7857–7863 (2005).
6. Leevy, W. M. *et al.* Noninvasive optical imaging of *Staphylococcus aureus* bacterial infection in living mice using a Bis-dipicolylamine-Zinc(II) affinity group conjugated to a near-infrared fluorophore. *Bioconjug. Chem.* **19,** 686–692 (2008).
7. Rouzet, F. *et al.* Technetium 99m-labeled annexin V scintigraphy of platelet activation in vegetations of experimental endocarditis. *Circulation* **117,** 781–789 (2008).
8. Boos, W. & Shuman, H. Maltose/maltodextrin system of *Escherichia coli*: Transport, metabolism, and regulation. *Microbiol. Mol. Biol. Rev.* **62,** 204–229 (1998).
9. Gopal, S. *et al.* Maltose and maltodextrin utilization by Listeria monocytogenes depend on an inducible ABC transporter which is repressed by glucose. *PLoS ONE* **5,** e10349 (2010).
10. Oldham, M. L., Khare, D., Quiocho, F. A., Davidson, A. L. & Chen, J. Crystal structure of a catalytic intermediate of the maltose transporter. *Nature* **450,** 515–521 (2007).
11. Brass, J. M., Bauer, K., Ehmann, U. & Boos, W. Maltose-binding protein does not modulate the activity of maltoporin as a general porin in *Escherichia coli*. *J. Bacteriol.* **161,** 720–726 (1985).
12. Lipsky, B. A., Itani, K. & Norden, C. Treating foot infections in diabetic patients: A randomized, multicenter, open-label trial of linezolid versus ampicillin-sulbactam/amoxicillin-clavulanate. *Clin. Infect. Dis.* **38,** 17–24 (2004).
13. Reiber, G. E., Pecoraro, R. E. & Koepsell, T. D. Risk factors for amputation in patients with diabetes mellitus. A case-control study. *Ann. Intern. Med.* **117,** 97–105 (1992).
14. Moore, E. H. Atypical mycobacterial infection in the lung: CT appearance. *Radiology* **187,** 777–782 (1993).
15. Erasmus, J. J., McAdams, H. P., Farrell, M. A. & Patz, E. F. Jr Pulmonary nontuberculous mycobacterial infection: Radiologic manifestations. *Radiographics* **19,** 1487–1505 (1999).
16. Dahl, M. K. & Manson, M. D. Interspecific reconstitution of maltose transport and chemotaxis in *Escherichia coli* with maltose-binding protein from various enteric bacteria. *J. Bacteriol.* **164,** 1057–1063 (1985).
17. Reuss, R. *et al.* Intracellular delivery of carbohydrates into mammalian cells through swelling-activated pathways. *J. Membr. Biol.* **200,** 67–81 (2004).
18. Line, B. R., Weber, P. B., Lukasiewicz, R. & Dansereau, R. N. Reduction of background activity through radiolabeling of antifibrin Fab′ with ^{99m}Tc-dextran. *J. Nucl. Med.* **41,** 1264–1270 (2000).
19. Demko, Z. P. & Sharpless, K. B. A click chemistry approach to tetrazoles by Huisgen 1,3-dipolar cycloaddition: Synthesis of 5-acyltetrazoles from azides and acyl cyanides. *Angew. Chem. Int. Ed. Engl.* **41,** 2113–2116 (2002).
20. Tornoe, C. W., Christensen, C. & Meldal, M. Peptidotriazoles on solid phase: [1,2,3]-triazoles by regiospecific copper(I)-catalyzed 1,3-dipolar cycloadditions of terminal alkynes to azides. *J. Org. Chem.* **67,** 3057–3064 (2002).
21. Dippel, R. & Boos, W. The maltodextrin system of *Escherichia coli*: Metabolism and transport. *J. Bacteriol.* **187,** 8322–8331 (2005).
22. Freundlieb, S., Ehmann, U. & Boos, W. Facilitated diffusion of p-nitrophenyl-alpha-D-maltohexaoside through the outer membrane of Escherichia coli. Characterization of LamB as a specific and saturable channel for maltooligosaccharides. *J. Biol. Chem.* **263,** 314–320 (1988).
23. Baba, T. *et al.* Construction of *Escherichia coli* K-12 in-frame, single-gene knockout mutants: the Keio collection. *Mol. Syst. Biol.* **2,** 2006.0008 (2006).
24. Reid, G. Biofilms in infectious disease and on medical devices. *Int. J. Antimicrob. Agents* **11,** 223–226 (1999).
25. Author, A. N. Panel discussion on biofilms in urinary tract infection. *Int. J. Antimicrob. Agents* **11,** 237–239 (1999).
26. Hall-Stoodley, L., Costerton, J. W. & Stoodley, P. Bacterial biofilms: From the natural environment to infectious diseases. *Nature Rev. Microbiol.* **2,** 95–108 (2004).
27. Kolodkin-Gal, I. *et al.* D-amino acids trigger biofilm disassembly. *Science* **328,** 627–629 (2010).
28. Dehoux, M. J., van Beneden, R. P., Fernandez-Celemin, L., Lause, P. L. & Thissen, J. P. Induction of MafBx and Murf ubiquitin ligase mRNAs in rat skeletal muscle after LPS injection. *FEBS Lett.* **544,** 214–217 (2003).
29. Luo, G., Niesel, D. W., Shaban, R. A., Grimm, E. A. & Klimpel, G. R. Tumor necrosis factor alpha binding to bacteria: evidence for a high-affinity receptor and alteration of bacterial virulence properties. *Infect. Immun.* **61,** 830–835 (1993).
30. Larson, T. J., Ludtke, D. N. & Bell, R. M. sn-Glycerol-3-phosphate auxotrophy of plsB strains of Escherichia coli: evidence that a second mutation, plsX, is required. *J. Bacteriol.* **160,** 711–717 (1984).

Acknowledgements

This project has been funded in whole or in part with Federal funds from the National Heart, Lung, and Blood Institute, National Institutes of Health, Department of Health and Human Services, under Contract No. HHSN268201000043C, NSF-BES-0546962 Career Award (N.M.) and NIH RO1 HL096796-01 (N.M.).

Author contributions

X.N. synthesized and characterized MDP-1 and MDP-2, designed and analysed experiments, and wrote the manuscript. S.L. designed, carried out and analysed experiments, and contributed to the writing of the manuscript. Z.W. performed MS experiments to characterize all intermediates and final products and proof read the manuscript. D.K. carried out *in vitro* experiments. B.S. prepared biofilms and performed confocal laser scanning microscopy. E.G. supervised the preparation of biofilms and proof read the manuscript. N.M. designed and supervised the project and contributed to the writing of the manuscript.

Additional information

The authors declare no competing financial interests. Supplementary information accompanies this paper on www.nature.com/naturematerials. Reprints and permissions information is available online at http://www.nature.com/reprints. Correspondence and requests for materials should be addressed to N.M.

© 2011 Macmillan Publishers Limited. All rights reserved